Antiferromagnetic ordering of organic Mott insulator λ-(BEDSe-TTF)$_2$GaCl$_4$

A. Ito,[1] T. Kobayashi,[1,*] D. P. Sari,[2,3] I. Watanabe,[3] Y. Saito,[4]
A. Kawamoto,[5] H. Tsunakawa,[1] K. Satoh,[1,†] and H. Taniguchi[1]

[1]*Graduate School of Science and Engineering, Saitama University, Saitama, 338-8570, Japan*
[2]*Innovative Global Program, College of Engineering, Shibaura Institute of Technology, Saitama 337-8570, Japan*
[3]*Advanced Meson Science Laboratory, RIKEN, Saitama 351-0198, Japan*
[4]*Institute of Physics, Goethe-University Frankfurt, 60438 Frankfurt (M), Germany*
[5]*Department of Condensed Matter Physics, Graduate School of Science, Hokkaido University, Sapporo 060-0810, Japan*

(Dated: May 13, 2022)

The band structure and magnetic properties of organic charge-transfer salt λ-(BEDSe-TTF)$_2$GaCl$_4$ (BEDSe-TTF: bis(ethylenediseleno)tetrathiafulvalene; abbreviated as λ-BEDSe) are investigated. The reported crystal structure is confirmed using X-ray diffraction measurements, and the transfer integrals are calculated. The degree of electron correlation U/W (U: on-site Coulomb repulsion, W: bandwidth) of λ-BEDSe is larger than one and comparable to that of the isostructural Mott insulator λ-(ET)$_2$GaCl$_4$ (ET: bis(ethylenedithio)tetrathiafulvalene, abbreviated as λ-ET), whereas the U/W of the superconducting salt λ-(BETS)$_2$GaCl$_4$ (BETS: bis(ethylenedithio)tetraselenafulvalene) is smaller than one. ^{13}C-NMR and μSR measurements revealed that λ-BEDSe undergoes an antiferromagnetic (AF) ordering below $T_{\rm N} = 22$ K. In the AF state, discrete ^{13}C-NMR spectra with a remaining central peak are observed, indicating the commensurate AF spin structure also observed in λ-ET. The similarity between the structural and magnetic properties of λ-BEDSe and λ-ET suggests that both salts are in the same electronic phase, i.e., the physical properties of λ-BEDSe can be understood by the universal phase diagram of bandwidth-controlled λ-type organic conductors obtained by donor molecule substitution.

I. INTRODUCTION

In molecular-based organic conductors, electronic properties are drastically changed by applying physical pressure. For example, (TMTSF)$_2$PF$_6$ (TMTSF: tetramethyltetraselenafulvalene) is a quasi-one-dimensional metal exhibiting a spin-density-wave ordering below 12 K [1], and κ-(BEDT-TTF)$_2$Cu[N(CN)$_2$]Cl [BEDT-TTF (ET): bis(ethylenedithio)tetrathiafulvalene (Fig. 1(a)-**i**)] is a quasi-two-dimensional Mott insulator exhibiting an antiferromagnetic (AF) ordering below 22.8 K [2–4]. However, they both show superconductivity under pressure [5, 6]. Therefore, it is believed that electron correlation plays a key role in the occurrence of superconductivity, and to this end, these systems have been well studied [7]. To understand the relationship between superconducting (SC) and adjacent electronic phases, each phase should be investigated in detail, and the pressure–temperature phase diagram should be established. For this purpose, chemical pressure can be applied using molecular substitution. Replacing anion molecules PF_6 with ClO_4 and Cu[N(CN)$_2$]Cl with Cu[N(CN)$_2$]Br or Cu(NCS)$_2$ results in a pressure effect, which leads to superconductivity under ambient pressure [8–10]. This approach greatly facilitates the understanding of superconductivity. Thus far, many unconventional properties have been reported [11].

λ-(BEDT-TSF)$_2M$Cl$_4$ [BEDT-TSF (BETS): bis(ethylenedithio)tetraselenafulvalene (Fig. 1(a)-**ii**), M = Ga, Fe] also exhibits interesting properties such as field-induced superconductivity [12], Fulde–Ferrell–Larkin–Ovchinnikov superconductivity [13–15], and an anisotropic SC gap [16–19]. Thus, they should be investigated in addition to the above-mentioned compounds. To investigate the mechanism of superconductivity in λ-type salts, the chemical pressure effect of substituting bromine for chlorine in λ-(BETS)$_2$GaCl$_4$ (abbreviated as λ-BETS) has been studied [20, 21]. With an increase in the amount of bromine, the spin-density-wave phase has been found to be adjacent to the SC phase [22]. However, in the system of λ-(BETS)$_2$GaBr$_x$Cl$_{4-x}$, the pressure range investigated by bromine substitution is narrow because λ-type salts can be obtained only in the range $x < 2$ [21] and superconductivity occurs at 0.12 GPa for $x = 1.5$ [23].

For complementary information on a wider pressure range, a universal phase diagram using donor molecular substitution has been proposed, as illustrated in Fig. 1(b) [24, 25]. As demonstrated by the substitution of TMTSF for TMTTF (tetramethyltetrathiafulvalene) [26], the substitution of S and Se in the TTF skeleton leads to a large pressure effect because of the significant change in the intermolecular transfer integrals. In fact, λ-(BEDT-STF)$_2$GaCl$_4$ [BEDT-STF (STF): unsymmetrical-bis(ethylenedithio)diselenadithiafulvalene (Fig.1(a)-**iii**); abbreviated as λ-STF], is an insulator at ambient pressure, and superconductivity emerges at a pressure of $\sim$ 1.3 GPa [24, 27], which confirms the universal phase diagram. λ-(ET)$_2$GaCl$_4$ (abbreviated as λ-ET), which is located at a more negative pressure side than

* tkobayashi@phy.saitama-u.ac.jp
† Deceased, 11 June 2021

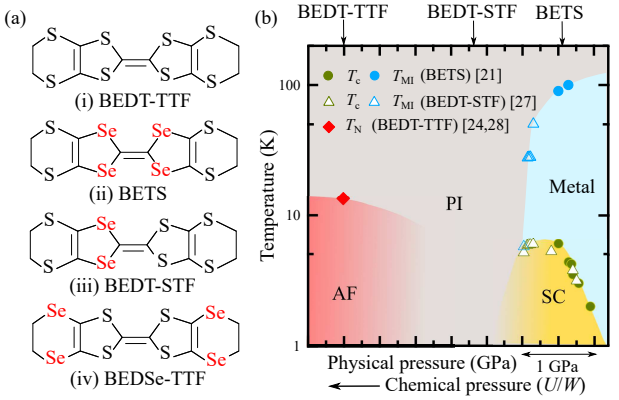

FIG. 1. (a) Molecular structure of (**i**)BEDT-TTF, (**ii**)BETS, (**iii**)BEDT-STF, and (**iv**)BEDSe-TTF. (b) Phase diagram of λ-D_2GaCl_4 (D = BEDT-TTF, BEDT-STF, BETS). T_c (green symbols) for SC transition and T_{MI} (blue symbols) for metal–insulator transition were determined from the resistivity measurements under pressure [21, 27]. The AF ordering temperature T_N (red rhombus) of λ-ET was obtained by a ^{13}C-NMR and electron-spin resonance measurements [24, 28].

λ-STF, undergoes a transition from a Mott insulator to an antiferromagnet at 13 K [28], whereas magnetic ordering is not observed in λ-STF [27, 29]. The absence of the magnetic order may be the quantum critical effect of λ-STF being located between the AF and SC phases [29] or the disorder effect originating from the asymmetric BEDT-STF molecules. In contrast, the AF order has been observed in λ-$(BETS)_2FeCl_4$ [30, 31] and λ-$(STF)_2FeCl_4$ [32–34], although there is a contribution of $3d$ spins from the Fe ions. Physical properties in λ-ET that do not contain asymmetry in its donor molecule should be investigated under pressure to understand why λ-STF does not exhibit any magnetic ordering. However, several polymorphs are obtained simultaneously in the synthesis of λ-ET, and the main product is δ-$(ET)_2GaCl_4$ [35–37], which complicates the study of the physical properties of λ-ET. Further, several polymorphs of $(ET)_2FeCl_4$ have been synthesized [38, 39], but the λ-type salt is not obtained.

To address the aforementioned problems, we focused on the BEDSe-TTF molecule shown in Fig. 1(a)-**iv**, where BEDSe-TTF denotes bis(ethylenediseleno)tetrathiafulvalene. Cui *et al.* reported the lattice parameters of λ-$(BEDSe\text{-}TTF)_2GaCl_4$ (λ-BEDSe) [40], which are larger than those of λ-ET, indicating a negative chemical pressure effect. The negative chemical pressure effect by BEDSe-TTF molecular substitution for an ET molecule was demonstrated in κ-$(ET)_2Cu[N(CN)_2]Br$ [41]. These results suggest that λ-BEDSe is a promising candidate to provide further information on the insulating phase of the universal phase diagram. Moreover, there are no reports of polymorphisms in either $(BEDSe\text{-}TTF)_2GaCl_4$ or $(BEDSe\text{-}TTF)_2FeCl_4$, which is a great advantage in investigating their physical properties. However, physical properties are yet to be reported for λ-BEDSe except for the semiconducting resistivity above 200 K [40].

In this study, we investigate the structural and magnetic properties of λ-BEDSe to explore whether it is located on the universal phase diagram and to promote the understanding of the insulating phase.

II. EXPERIMENTAL

Single crystals of λ-BEDSe were prepared by the electrochemical oxidation of BEDSe-TTF in a solution of chlorobenzene containing 10 % ethanol with tetrabutylammonium salt of $GaCl_4^-$. The samples were needle-like crystals as in the other λ-type salts. Polymorphism was not confirmed in our experiments unlike for other λ-type salts.

Single-crystal X-ray diffraction measurements on λ-D_2GaCl_4 (D = BEDSe-TTF, ET, and BETS) were performed using a Bruker SMART APEX2 diffractometer by employing a graphite-monochromated Mo-K_α radiation (λ = 0.71073 Å) at the Comprehensive Analysis Center for Science, Saitama University, Japan. The diffraction data were collected at 110 K, and the structures were solved using SHELXT [42] and refined using SHELXL [43].

The overlap integrals, band dispersion, and Fermi surface were obtained by the tight-binding calculation based on the extended Hückel method [44]. The transfer integrals t were estimated from the overlap integrals S assuming that $t = ES$, where E represents a constant of -10.0 eV. For Se-containing organic conductors, the choice of the Hückel parameters for the Se atom remain controversial [45, 46]. Mori and Katsuhara studied the parameter dependence of the overlap integrals in λ-type salts, and in this study, we applied the same parameter set [47, 48].

Magnetization measurements on λ-BEDSe were performed using a superconducting quantum interference device magnetometer (Quantum Design MPMS XL-7). The magnetic susceptibility of polycrystalline samples with a weight of 7.9 mg was measured under a magnetic field of 1 T between 2 and 300 K. The spin susceptibility was acquired by subtracting the core diamagnetic contribution of -5.00×10^{-4} emu/mol estimated from the measured susceptibility of ingredients such as neutral molecules.

Muon-spin rotation (μSR) experiments on λ-BEDSe were carried out using a general purpose surface-muon instrument at Swiss Muon Source (SμS), Paul Scherrer Institut (Villigen, Switzerland). We used a continuous muon beam with the spin polarization parallel to the beamline. A randomly oriented polycrystalline sample of 50 mg was wrapped in silver foil. Measurements were conducted under zero magnetic field at temperatures between 40–1.6 K to cover the temperature range of the magnetic transition.

For a ^{13}C NMR experiment, we prepared ^{13}C enriched

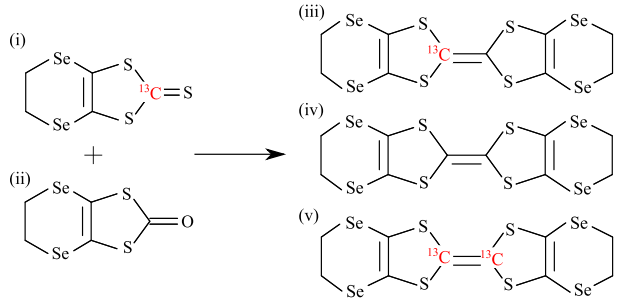

FIG. 2. Synthesis of ^{13}C enriched BEDSe-TTF molecules.

TABLE I. Lattice parameters for λ-D_2GaCl$_4$ (D = BEDSe-TTF, ET, and BETS).

Parameter	λ-BEDSe	λ-ET	λ-BETS
a (Å)	16.1260(14)	15.9661(15)	15.9166(19)
b (Å)	18.1099(15)	17.9068(17)	18.451(2)
c (Å)	6.6519(6)	6.4544(6)	6.5435(8)
α (°)	97.397(1)	98.520(1)	98.606(1)
β (°)	97.154(1)	96.731(2)	95.960(1)
γ (°)	111.886(1)	112.027(2)	112.261(1)
V (Å^3)	1755.9(3)	1661.4(3)	1731.2(4)

BEDSe-TTF molecules synthesized from ^{13}C enriched thioketone (**i**) and cool ketone (**ii**) (Fig. 2) [49], as used in the preparation of the single-site ^{13}C-enriched ET molecule [50, 51]. This cross coupling afforded 78 % of (**iii**), 18 % of (**iv**), and 4 % of (**v**). Their ratio was estimated from the cross-coupling reaction of deuterated thioketone (**i**) and cool ketone (**ii**) using mass spectroscopy. As molecule (**iv**) is NMR inactive, the NMR signals were obtained from the molecule (**iii**), which helped prevent the Pake doublet problem [52]. ^{13}C-NMR experiments were performed for a single crystal with dimensions of $10 \times 0.35 \times 0.04$ mm^3 in a magnetic field of 6 T parallel to the long axis of the BEDSe-TTF molecules, where the NMR shift becomes minimum in the a^*b^* plane. The NMR spectra were obtained by the fast Fourier transformation of the spin-echo signals with a $\pi/2$-π pulse sequence. The typical $\pi/2$ pulse length was 2 μs. Spin-lattice relaxation time T_1 was measured by a conventional saturation-recovery method.

III. RESULTS AND DISCUSSION

A. Crystal structure

The structural analyses of λ-D_2GaCl$_4$ (D = BEDSe-TTF, ET, and BETS) were performed at 110 K because crystallographic data including atomic parameters were not reported in previous papers [24, 40]. This information is useful not only for comparing the structure but also for performing band structure calculations. Table I shows the lattice parameters of the three salts. Results are consistent with those previously reported [21, 24, 40]. These values show that the three salts are isostructural, which indicates that physical properties can be understood by the same phase diagram. From a comparison of the three salts, the unit cell volumes of λ-BETS and λ-BEDSe are larger than that of λ-ET by 4.2 % and 5.7 %, respectively. This implies that the replacement of S atoms with Se atoms in the ET molecule leads to lattice expansion. In addition, the unit cell volume of λ-BEDSe is larger than that of λ-BETS, which shows that the substitution at the outer chalcogen atoms has a greater effect on the lattice expansion. These lattice expansions are considered the negative chemical pressure effect; however, λ-BETS and λ-BEDSe are metallic and insulating, respectively. To discuss the actual pressure effect, not only the lattice constants but also the intermolecular overlap integrals should be investigated.

TABLE II. Interplanar and sliding distances in the overlap mode between molecules for λ-D_2GaCl$_4$ (D = BEDSe-TTF, BEDT-TTF, and BETS).

Modes	λ-BEDSe	λ-ET	λ-BETS
Interplanar distance			
I–II	3.57	3.49	3.83
I–I*	4.00	3.99	4.15
II–II*	4.51	4.11	4.02
Sliding distance			
I–II	1.00	0.99	1.20
I–I*	2.82	2.68	2.84
II–II*	4.80	4.71	4.76

Figure 3(a)–(c) show the crystal structure of λ-BEDSe. In this system, BEDSe-TTF layers and GaCl$_4$ layers are alternately stacked along the b axis [Fig. 3(a)]. In the BEDSe-TTF layers, there are two crystallographically independent molecules: I (I*) and II (II*), where molecules marked with asterisks are related to the unmarked ones by the inversion center. These molecules are stacked along the a axis [Fig. 3(b)]; however, the overlap modes characterized by sliding distance along the long axis of the molecule [Fig. 3(c)] and interplanar distance between the molecules are different. Table II shows that these values between molecules I and II are smaller than the others and are close to that of κ-type salts (sliding distance is 1.59 Å and interplanar distance is 3.56 Å) [53], which suggests molecules I and II form a dimer.

Among the three salts, interplanar distances are significantly different whereas the sliding distances are insignificant (Table II). These differences affect the magnetic interaction between dimers, as discussed in Sec. III C.

B. Band structure calculation

We performed tight binding calculations for λ-D_2GaCl$_4$ (D = BEDSe-TTF, ET, and BETS) using the

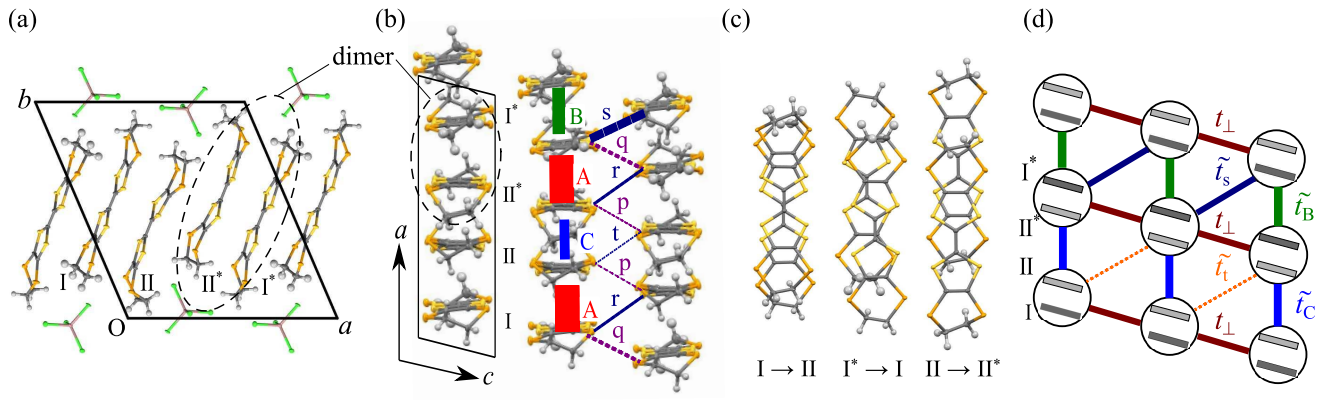

FIG. 3. (a) Layered crystal structure of λ-BEDSe viewed along the c axis. (b) In-plane structure of the BEDSe-TTF layer in the ac plane. Square and dotted ellipse represent the unit cell and dimer of the BEDSe-TTF molecules, respectively. (c) Overlaps between each molecule viewed perpendicular to the molecular plane. (d) Schematic representation of the BEDSe-TTF layer in a dimer model, where circles represent dimers.

TABLE III. Transfer integrals t ($\times 10^{-3}$ eV) [Fig. 3(b)] of λ-D_2GaCl$_4$ (D = BEDSe-TTF, BEDT-TTF, and BETS).

Parameter	λ-BEDSe	λ-ET	λ-BETS
t_A	304.8	282.1	360.4
t_B	−122.7	−83.92	−179.2
t_C	−130.9	−90.63	−156.0
t_p	20.04	22.01	30.51
t_q	55.50	46.63	99.21
t_r	55.68	62.35	123.7
t_s	−121.3	−132.9	−173.2
t_t	−24.84	−16.56	−25.78

obtained atomic parameters. Table III shows the transfer integrals of the three salts, and the definitions are displayed in Fig. 3(b). As inferred from the overlap modes of the crystal structure, t_A is significantly larger than t_B and t_C, which indicates that molecules I and II form a dimer from the perspective of electronic structure.

The magnitude of the transfer integrals along the stack direction for λ-BEDSe is intermediate between those for λ-ET and λ-BETS. In contrast, the transfer integrals perpendicular to the stack directions are not significantly different between λ-ET and λ-BEDSe, and they are smaller than those for λ-BETS. In the BEDT-TTF molecule, the electron densities of the inner chalcogen atoms are greater than those of the outer ones. Considering that the chalcogen atom in the TTF skeleton of λ-BEDSe and λ-ET is sulfur and that of λ-BETS is selenium, transfer integrals perpendicular to the stack directions are dominated by the orbital overlap of inner chalcogen atoms, whereas the outer chalcogen atoms contribute to the transfer integrals along the stack direction.

From these transfer integrals, the band dispersion and

TABLE IV. Upper part shows U and W ($\times 10^{-3}$ eV), and the ratio of U to W for λ-D_2GaCl$_4$ (D = BEDSe-TTF, BEDT-TTF, and BETS). The lower part shows the ratio of the transfer integrals of the dimer model $\tilde{t}_\nu$ (ν: B, C, s, and t) to that of $t_\perp$ [Fig. 3(d)].

Parameter	λ-BEDSe	λ-ET	λ-BETS
U	609.6	564.2	720.8
W	500.4	449.0	809.1
U/W	1.218	1.256	0.891
$\lvert\tilde{t}_B/t_\perp\rvert$	0.935	0.641	0.707
$\lvert\tilde{t}_C/t_\perp\rvert$	0.998	0.692	0.616
$\lvert\tilde{t}_s/t_\perp\rvert$	0.924	1.015	0.683
$\lvert\tilde{t}_t/t_\perp\rvert$	0.189	0.126	0.102

Fermi surface of λ-BEDSe were obtained as shown in Fig. 4. The band dispersion is split into the upper and lower bands as in the case of λ-ET and λ-BETS because of the dimerized structure [21, 24, 28]. The overlapped single Fermi surface is disconnected because of the anisotropic transfer integral lattice. The Fermi surface consists of a two-dimensional cylindrical part and a one-dimensional flat part. These features are the same among all three salts.

Based on the discussion proposed by Hotta [54], we estimate the electron correlation by considering the transfer integrals of λ-type salts in the dimer model. The transfer integrals in the dimer model are defined as $\tilde{t}_B \equiv t_B/2$, $\tilde{t}_C \equiv t_C/2$, $\tilde{t}_s \equiv t_s/2$, $\tilde{t}_t \equiv t_t/2$, and $t_\perp \equiv (t_p + t_q + t_r)/2$ [see Fig. 3(d)]. Here, $t_\perp$ should be calculated carefully because the sign of the transfer integral between the dimers must be considered properly. In our calculation, the phase of the highest occupied molecular orbital is taken so that the intra-dimer over-

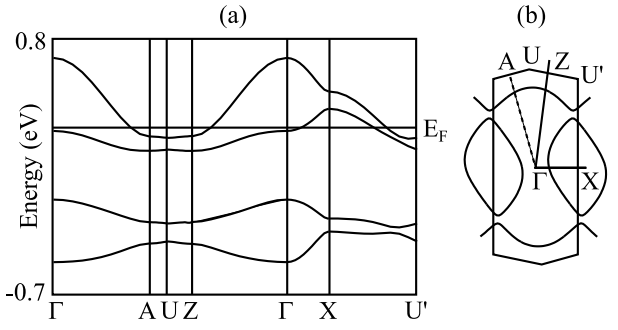

FIG. 4. (a) Band structure and (b) Fermi surface of λ-(BEDSe-TTF)$_2$GaCl$_4$.

lap is negative, resulting in $t_A > 0$. As the hole resides on the antibonding molecular orbital in the dimer, the phase factor between the inter-dimer orbital corresponds to that used in the calculation; i.e., $t_\perp = (t_p + t_q + t_r)/2$. Note that when the hole is on the bonding orbital, the phase of one of the molecules must be reversed, resulting in $t_\perp = (t_p + t_q - t_r)/2$.

The on-site Coulomb repulsion energy is approximately proportional to the transfer integral within the dimer in a dimeric structure, i.e., $U = 2t_A$ [55, 56]. The bandwidth W is estimated according to the relation [54]

$$W = \sum_\nu \tilde{t}_\nu + 4t_\perp + \frac{(\sum_\nu \tilde{t}_\nu)^2}{16t_\perp}, \qquad (1)$$

where ν represents B, C, s, and t. Further, the U, W, and U/W parameters of each salt calculated by these definitions are listed in the top part of Table IV. The three salts are situated at $U/W \sim 1$, indicating that they are in a region where itinerancy and localization are in competition. The U/W parameters of λ-BEDSe and λ-ET are nearly the same and greater than 1, and that of λ-BETS is significantly less than 1. These results suggest that λ-BEDSe and λ-ET are more localized than λ-BETS, and that there is a Mott transition between the two salts and λ-BETS. These observations are consistent with experimental facts about the conductivity of λ-type salts [24].

C. Spin susceptibility

Figure 5 shows the temperature dependence of spin susceptibility χ_{spin} of λ-BEDSe. As the temperature is reduced from 300 K, χ_{spin} increases towards 100 K, where it shows a broad maximum. Further decreasing temperature, χ_{spin} decreases to 22 K. The broad maximum of χ_{spin} is a characteristic of a system possessing a low-dimensional magnetic interaction network.

For λ-ET and λ-STF, the temperature dependence of χ_{spin} have been discussed using the two-dimensional (2D) Heisenberg AF spin model [57, 58]. Interestingly, the

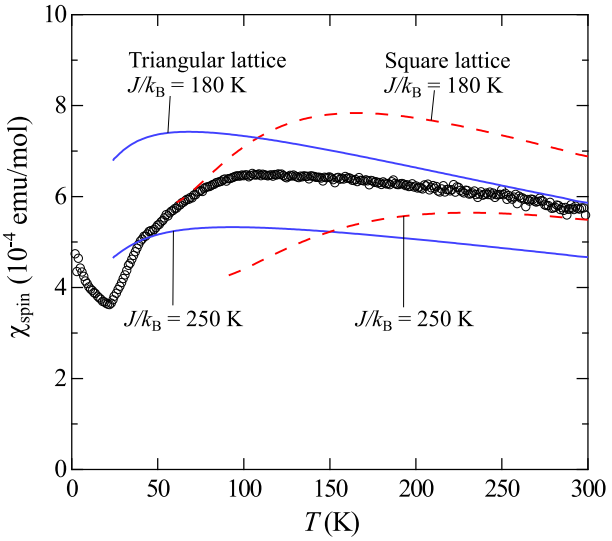

FIG. 5. (a) Temperature dependence of spin susceptibility of λ-BEDSe. Blue solid lines represent the 2D Heisenberg AF triangular-lattice model [57], and the red dashed lines represent the 2D Heisenberg AF square-lattice model [58].

χ_{spin} of λ-ET and λ-STF have been explained by the square and triangular lattice models, respectively [27–29]. Here, we applied these analyses to λ-BEDSe. The solid and dashed lines in Fig. 5 show the temperature dependencies of χ_{spin} assuming the triangular and square lattice AF spin models, respectively. As a rough estimation of the exchange interaction J, the calculation results for $J/k_B = 180$ K and 250 K are shown, which are the upper and lower limits; here, the experimental data above ~ 50 K are included. Both models do not reproduce the experimental result.

Considering the network of J between the dimers in λ-BEDSe, we can speculate why the experimental result cannot be explained by these models. Because J is expressed as $J = 4t^2/U$ in the case of localized systems, we discuss the network of J using the transfer integrals relative to $|t_\perp|$, as shown in Table IV. The transfer integrals other than $|\tilde{t}_t|$ are comparable to $|t_\perp|$, and $|\tilde{t}_t|$ is negligibly small. Thus, the network of the transfer integrals in λ-BEDSe is a combination of a triangular ladder and a squared ladder, which is similar to the so-called trellis lattice discussed in Ref. [59] [see Fig. 3(d)]. This result is consistent with the result of spin susceptibility because the temperature of the broad peak of χ_{spin} is roughly intermediate between those of the triangular and square lattice AF spin models. Further calculations are required to verify whether the spin model of the lattice can explain the experimental results.

Although λ-ET and λ-STF have almost the same structure as λ-BEDSe, the simple square and triangular lattice AF spin models can reasonably explain the temperature dependence of the χ_{spin} of λ-ET and λ-STF. A possible reason for this is the difference in the network of J be-

tween the three salts. There is actually a difference in the overlap modes in λ-BEDSe, λ-ET, and λ-BETS (Table II). $|\tilde{t}_B/t_\perp|$ and $|\tilde{t}_C/t_\perp|$ for λ-ET are smaller than those for λ-BEDSe. When $|\tilde{t}_s|^2$ and $|t_\perp|^2$, being twice as large as $|\tilde{t}_B|^2$ and $|\tilde{t}_C|^2$, are dominant in the network of J, we can approximate λ-ET as a square lattice, which is consistent with the experimental results of χ_{spin} [28]. For λ-STF, the transfer integrals are difficult to evaluate because of the molecular asymmetry of BEDT-STF. However, the difference in the network of J between λ-ET and λ-BETS suggests that the network of J in λ-STF is also different. Further, because line broadening of the ^{13}C-NMR spectra has been observed in λ-STF [29], there is a possibility of charge disproportionation, which can modify the transfer integrals between the molecules. These features may be responsible for the temperature dependence of the triangular lattice-like χ_{spin} in λ-STF.

In this study, we systematically evaluated the magnitude of the relative transfer integrals in the dimer model to investigate the network of J. Note that the relative transfer integrals depend on the calculation method and the Hückel parameters [60–62]. At least, a small $\tilde{t}_t$ is a characteristic behavior of λ-type salts, and the lattice realized by neglecting $\tilde{t}_t$ is considered to be the fundamental model for discussing the spin structure of λ-type salts. In this context, λ-BEDSe would be a useful reference material for discussing the magnetism of λ-type salts.

Below 22 K, χ_{spin} increases, while the magnitude of the increase is not as drastic as that observed in canted antiferromagnet κ-$(ET)_2Cu[N(CN)_2]Cl$ [2, 63]. This can be attributed to the small amounts of magnetic impurities and/or magnetic transition where an anisotropy of magnetic susceptibility appears. To clarify the magnetic state at low temperatures, microscopic measurements should be conducted. As another anomaly, a small kink structure was observed at approximately 40 K. This is a small change in slope and is observed in data extracted from preliminary magnetic torque measurements. Thus, although it may be intrinsic, its origin is unknown at this stage.

D. μSR

A μSR measurement can be used for the sensitive detection of magnetic ordering to probe the magnetic state of λ-BEDSe microscopically at low temperatures. Figure 6(a) shows the time evolution of the muon-spin polarization (μSR time spectra) at several temperatures under a zero magnetic field. The μSR time spectra remain unchanged above 23.4 K, below which the relaxation rate becomes larger and clear precession signals are observed, confirming a magnetic ordering. To understand the observed μSR time spectra in detail, we analyze them separately for the paramagnetic and ordered phases as follows.

In the paramagnetic state above 23.4 K, the μSR time spectra can be fitted by

$$A(t) = Ae^{-\lambda t}G_{KT}(t) + A_{bg}, \quad (2)$$

where A and A_{bg} represent the relative ratios of amounts of the muons stopped inside the sample and in the silver sample holder, respectively, and λ is the relaxation rate. $G_{KT}(t)$ represents the Kubo–Toyabe function expressed as

$$G_{KT}(t) = \frac{1}{3} + \frac{2}{3}\left(1 - \Delta^2 t^2\right)\exp(-\frac{1}{2}\Delta^2 t^2), \quad (3)$$

where Δ represents the distribution width of the depolarization rate of the nuclear spin contribution.

In the ordered state, the main precession signals with a period of approximately 2 μs and a kink at around 0.5 μs were observed, although the latter is of small amplitude. To explain these μSR time spectra, we fitted them using the function

$$A(t) = A_0e^{-\lambda_0 t} + A_1\cos(\gamma_\mu B_{\mu_1} t + \phi)e^{-\lambda_1 t} + A_2\cos(\gamma_\mu B_{\mu_2} t + \phi)e^{-\lambda_2 t} + A_{bg}. \quad (4)$$

Here A_i and λ_i $(i = 0, 1, 2)$ represent the initial asymmetries and relaxation rates, respectively. A_{bg} was determined at a low temperature and fixed to 6.4 % both in the paramagnetic and ordered state. γ_μ, B_{μ_1}, and B_{μ_2} are the muon gyromagnetic ratio and the internal magnetic fields at the muon sites, respectively. ϕ is the phase of muon-spin precession determined by the transverse μSR measurement under 20 G at 40 K. The experimental data can be well reproduced by these fitting functions, as shown in Fig. 6(a); this indicates that there are two major muon sites.

The plot of B_{μ_2} against B_{μ_1} shown in Fig. 6(b) indicates that they are proportional to each other. This result strongly suggests that the two observed rotational components correspond to the muons stopped at magnetically inequivalent sites and that the development of the magnetic moment is observed from different muon sites. We discuss the positions of the two muon sites from the density functional theory (DFT) calculations performed within the Kohn–Sham approach using the projector augmented-waves formalism in the Vienna Ab-initio Simulation Packages (VASP) program [64, 65]. The exchange–correlation function generalized gradient approximation, GGA-PW91, was used [66]. The ground-state charge densities were calculated by adopting the value of the crystal axis obtained in Sec. III A, and by using the $4 \times 4 \times 4$ k-point sampling, ultrasoft pseudopotentials, and plane-wave densities. The calculations were performed on the HOKUSAI supercomputer. Figure 7 shows the crystal structure of λ-BEDSe and the electric minimum potential with the isosurface of 37.8 eV shown in cyan. Although there are several possible muon sites, we found two major sites: M_1 near $GaCl_4$, and M_2 near the ethylene groups. If the spin density is larger near the ethylene edge, it is likely that M_1 and M_2 are related

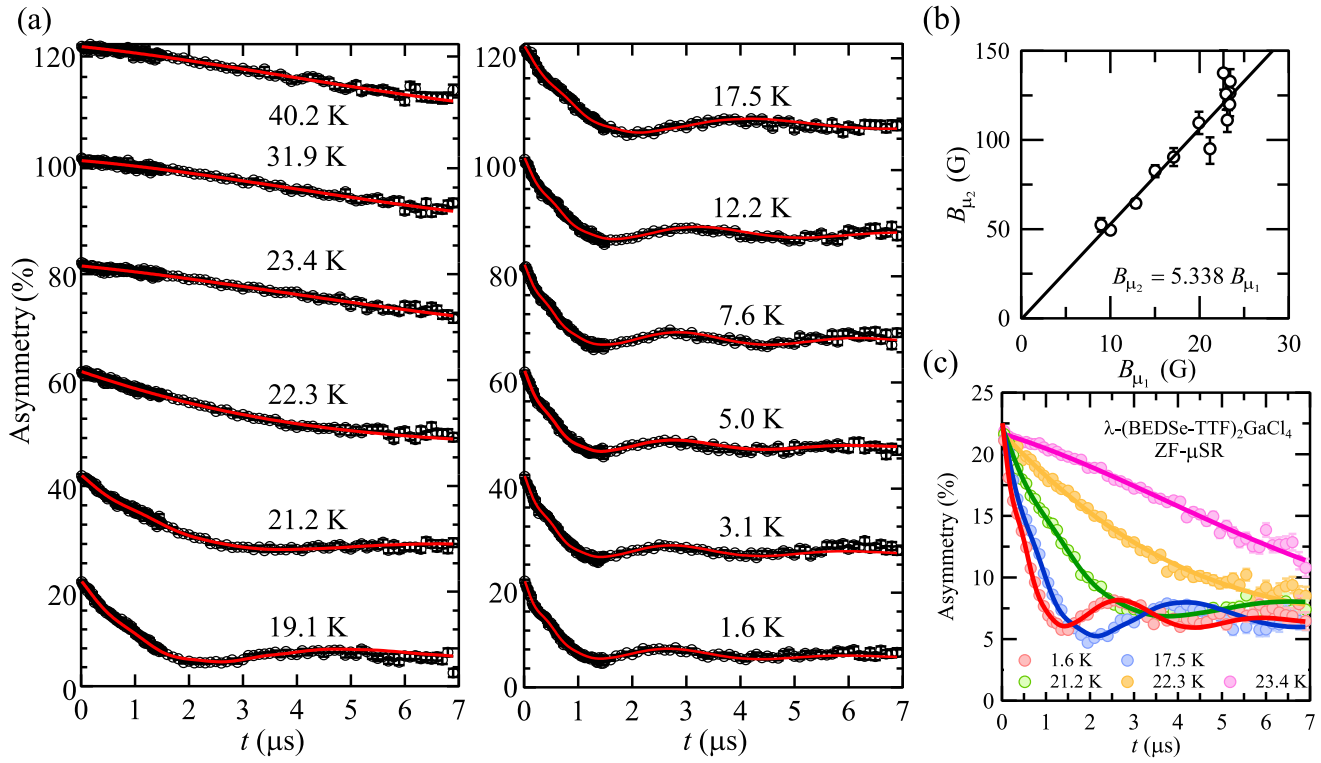

FIG. 6. (a) Temperature evolution of μSR time spectra at zero magnetic field. Each spectrum is vertically shifted by 20 % for ease of comparison. Solid curves represent the fitting results obtained using Eq. (2) ($T \geq 23.4$ K) and Eq. (4) ($T \leq 22.3$ K). (b) Relationship between B_{μ_1} and B_{μ_2} with the linear fitting. (c) Representative μSR time spectra. Solid lines are the fitting results when $B_{\mu_2} = 5.338 B_{\mu_1}$ in Eq. (4).

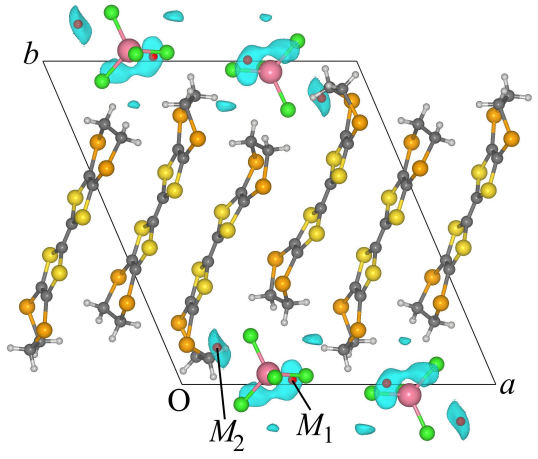

FIG. 7. Crystal structure of λ-BEDSe, and electric minimum potential with isosurface of 37.8 eV shown in the cyan region. The most possible muon stopping sites are marked in red.

to B_{μ_1} and B_{μ_2}, respectively. Although λ-BEDSe has a complex crystal structure, the major two muon sites observed in the present study can be consistently explained by the DFT calculations.

Here, to obtain more accurate fitting results, we fitted the μSR time spectra again using the relationship $B_{\mu_2} = 5.338 B_{\mu_1}$ obtained by the linear fitting of B_{μ_1} versus B_{μ_2}. Representative results of the fitting are shown in Fig. 6(c), together with that of the paramagnetic phase. The results of the fitting parameters are shown in Fig. 8. Figure 8(a) shows the temperature dependence of the initial asymmetry. The initial asymmetry is 15 % in the paramagnetic state, and it is distributed to each component by magnetic ordering; their total is 17 % in the AF state. Despite the different fitting functions below and above the magnetic ordering, the result of the almost unchanged total initial asymmetry verifies the validity of the analysis.

We discuss the volume fraction of long-range order based on the observed precession signals and total asymmetry below T_N. When a muon stops at a particular site in a long-range ordered state, 2/3 of the muon spins precess, and the remaining 1/3 do not because muons precess along one direction of the magnetic field. As shown in Fig. 8(a), the precession components are $A_1 + A_2 \sim 6$ %,

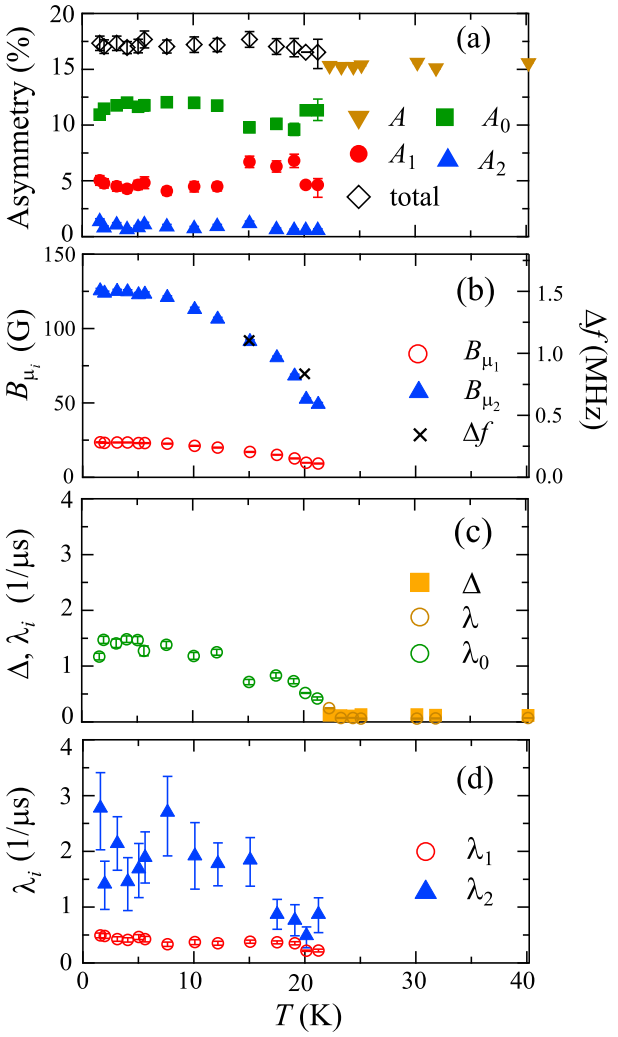

FIG. 8. Temperature dependence of the parameters obtained by fitting the μSR time spectra: (a) Initial asymmetry, (b) internal fields at muon sites (left axis), (c) relaxation rates λ and λ_0 and distribution width of the depolarization rate of the nuclear spin contribution Δ, and (d) relaxation rates λ_1 and λ_2. Splitting widths of the NMR spectra Δf in the AF state [defined in Fig. 9(a)] are plotted in panel (b) with the right axis.

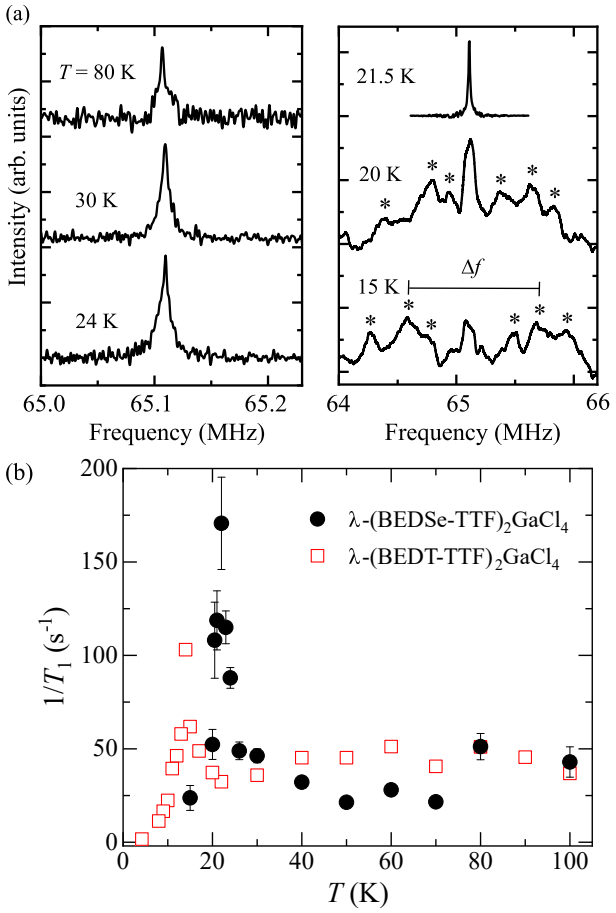

FIG. 9. (a) ^{13}C NMR spectra at several temperatures. The asterisks and Δf indicate the splitting peaks and the width of the second peaks from outside, respectively. (b) Temperature dependence of T_1^{-1} of λ-BEDSe and λ-ET [28].

and therefore, the fraction of muon spins undergoing internal magnetic fields in the long-range ordered state is 6 % $\times$ 3/2 = 9 %. Since the total asymmetry is 17 %, the volume fraction of the magnetic ordered component is 9/17 $\sim$ 53 %. This is the lower limit estimated from the analysis, and the actual volume fraction is expected to be much larger because there are other minor muon sites shown in Fig. 7; A_0 is also considered to include components derived from long-range order even though they cannot be analyzed as precession signals.

The internal fields and relaxation rates increase with decreasing temperature [Fig. 8(b) and (d)]. At sufficiently low temperatures below T_N, the increase in the internal magnetic field is saturated, which is a characteristic of the change in the order parameter of the magnetic transition. The extrapolated values of the two internal magnetic fields at 0 K are 125 G and 23.4 G, respectively, and they are comparable to those of a typical organic antiferromagnet κ-(ET)$_2$Cu[N(CN)$_2$]Cl [4]. The relaxation rate λ_0 increases below 22 K [Fig. 8(c)] as well as the other rotational components. The value $\lambda_0 = 1.5\ \mu s^{-1}$ estimated from Fig. 8(c) at the lowest temperature is equivalent to the magnetic field $B = 17.6$ G, which is comparable to the value of B_{μ_1}. This implies that the first term of Eq. (4) is from the same origin as the other rotational components.

E. NMR

In the NMR experiments, microscopic properties are probed similar to that in the μSR measurements. In addition, magnetic fluctuations can be detected from the T_1 measurement, which provides important insights into the

nature of the magnetic state. The ^{13}C-NMR method by ^{13}C substitution of C=C atoms in the center of the TTF skeleton is a powerful method to investigate the electronic state, as has been established for the BEDT-TTF salts. To conduct ^{13}C-NMR measurements for λ-BEDSe, we synthesized ^{13}C enriched BEDSe-TTF molecules, as described in Sec. II. To the best of our knowledge, this is the first ^{13}C-NMR measurement for BEDSe-TTF salts.

Figure 9(a) shows the temperature evolution of the NMR spectra. In the paramagnetic state, a single peak was observed. As λ-BEDSe has crystallographically independent BEDSe-TTF molecules I and II, each of which has two inequivalent ^{13}C sites, four peaks are expected. In the present experiment, a magnetic field was applied in the direction of the long axis of the BEDSe-TTF molecule, where the hyperfine coupling constant is small. As a result, the difference in the hyperfine coupling constants of each ^{13}C site becomes small, resulting in a single overlapping spectrum. Reflecting the presence of multiple ^{13}C sites, the spectrum at 80 K is not simply Lorentzian but shows a shoulder-like structure. With decreasing temperature, the structure of the spectrum becomes less pronounced, but the general shape remains almost unchanged in the paramagnetic state above 24 K.

The temperature dependence of T_1^{-1} is shown in Fig. 9(b). Because the spectrum consists of four peaks with slightly different hyperfine coupling constants, T_1 was determined by fitting the recovery of spin magnetization $M(t)$ using a stretched exponential function, $1 - M(t)/M(\infty) = \exp[-(t/T_1)^{\beta}]$, where $M(\infty)$ is the equilibrium spin magnetization at time $t \to \infty$ and β is the stretched exponent. The recovery curves could be fitted by $\beta = 0.9$ for all temperatures. At high temperatures far above $T_{\rm N}$, T_1^{-1} is constant as expected in a system with localized spins, indicating that the electronic state can be understood as a Mott insulator. Below 26 K, T_1^{-1} drastically increases towards $T_{\rm N} \simeq 22$ K because of the critical slowing down, which evidences a second-order phase transition. For comparison, the temperature dependence of T_1^{-1} of λ-ET are also plotted in Fig. 9(b) [28]. The magnitude of T_1^{-1} can be quantitatively compared because both experiments were performed under almost the same magnetic field direction and intensity and because the adjacent chemical environments around the central C=C atoms are the same between BEDSe-TTF and BEDT-TTF molecules. The absolute values of T_1^{-1} at high temperatures between both salts are comparable. As the values of T_1^{-1} at high temperatures correlate with the magnitude of the exchange interaction, the present results indicate that exchange interactions of λ-ET and λ-BEDSe are similar in order, although the lattice models may be different as discussed in Sec. III C.

Below 20 K, a drastic spectral splitting was observed, and this confirms the development of an internal magnetic field attributed to the magnetic ordering, which is consistent with the results of the μSR measurements. The spectrum consists of a central peak and three symmetrically discrete spectra from the central peak. Here, the discrete peaks are depicted by asterisks. These results suggest that the spin structure is commensurate. The commensurate spin structure with the central peak was similarly observed in λ-ET [28], indicating that the AF spin structures between both salts are the same, although the different networks of J are evaluated. The T_1 measurements in the AF state are performed on the central peak. T_1^{-1} decreases steeply below 22 K because of the decrease in the population of magnon excitations with decreasing temperature.

Analysis of the μSR spectra shows that the lower limit of the volume fraction of the long-range order is approximately half. However, the NMR measurements show that $1/T_1$ decreases steeply below $T_{\rm N}$ even in the central peak, suggesting that λ-BEDSe exhibits an almost 100 % long-range AF order. The $T_{\rm N} = 22$ K estimated by the NMR measurements is the same as the zero-field $T_{\rm N}$ estimated by the μSR measurements. From the field-independent $T_{\rm N}$ and absence of weak ferromagnetic behavior as discussed in Sec. III C, we suggested that no physical properties derived from the Dzyaloshinskii–Moriya interaction were observed, which would be expected when there is no inversion center between dimers as in κ-(ET)$_2$Cu[N(CN)$_2$]Cl [67, 68].

By further decreasing the temperature to 15 K, the spectral splitting is broadened. Among the six symmetrically discrete peaks, the width between the most intense peaks was defined as Δf [right side of Fig. 9(a)]. To discuss the development of the internal magnetic field with decreasing temperature, their values at 15 and 20 K are shown in Fig. 8(b). As the temperature dependence of the internal magnetic field observed at muon sites should be the same as that observed in NMR, the spectral splitting extrapolated to 0 K is estimated to be ~ 1.5 MHz. The splitting width of λ-ET is approximately 0.6 MHz [28], which is 2.5 times smaller than that of λ-BEDSe. Although the accurate ratio is difficult to obtain because of the broadness of the spectrum, the difference in the splitting width seems to correlate with the difference in $T_{\rm N}$.

F. Comparison of λ-ET and λ-BEDSe

The present study demonstrated that λ-BEDSe has almost the same value of U/W as λ-ET. Furthermore, the behavior of the NMR spectrum and T_1^{-1} is qualitatively the same between λ-BEDSe and λ-ET, although the AF spin model inferred from the temperature dependence of $\chi_{\rm spin}$ is different.

In addition, there is a significant difference in $T_{\rm N}$. $T_{\rm N} = 22$ K for λ-BEDSe is 1.7 times larger than $T_{\rm N} = 13$ K for λ-ET. The J of λ-BEDSe and λ-ET were estimated to be $J/k_B \sim 180$–250 K and $J/k_B \sim 98$ K [28] when the temperature dependence of $\chi_{\rm spin}$ is modeled by the 2D Heisenberg AF spin models. These results simply suggest that $T_{\rm N}$ is approximately proportional to J. The large difference between $T_{\rm N}$ and J/k_B in both salts suggest

that a very weak interlayer interaction may suppress T_N. In the case of quasi-2D Heisenberg antiferromagnets, the relationship between T_N and the intralayer and interlayer interactions have been discussed theoretically [69]. The results suggest that the interlayer interaction of both λ-ET and λ-BEDSe is far less than $J/1000$. Further, the literature also predicts that changes in T_N are sensitive to changes in intralayer interactions but insensitive to changes in interlayer interactions in cases where the interaction is extremely anisotropic. Therefore, even if the interlayer interactions were significantly different between the two salts within a sensible range, the twofold difference in T_N cannot be explained, and we conclude that it is because of the difference in the intralayer interactions. Another possibility is that a frustration effect may suppress the T_N in this series of the salts. Although this effect cannot be completely ruled out because λ-BEDSe has a partially triangular lattice as described above, this effect would not explain the difference in T_N even if there were a frustration effect.

Here, we discuss the relative positions of λ-BEDSe and λ-ET in the universal phase diagram. U/W is the primary parameter that should be considered; however, we cannot determine the relative positions from the U/W values of λ-ET and λ-BEDSe, between which there is no significant difference. The electrical resistivity measurements in κ-(BEDSe-TTF)$_2$Cu[N(CN)$_2$]Br indicate that the substitution of BEDT-TTF for BEDSe-TTF molecules has a negative pressure effect of approximately 0.15 GPa [41]. However, the analogy of the pressure effect from the results of κ-salt may be inappropriate because the molecular arrangement between the λ and κ phases is different. Therefore, we discuss the position in the universal phase diagram from the change in T_N with pressure. ^{13}C-NMR experiments have been performed on λ-ET under pressure, which suggest that T_N decreases rapidly to 3 K when a pressure of 0.4 GPa is applied [70]. Considering this result and the fact that λ-ET and λ-BEDSe could be located in the same electronic phase, λ-BEDSe, possessing a higher T_N than λ-ET, is located further to the negative pressure side. On the other hand, the electronic states of λ-ET under further pressure have not been detailed because of the existence of polymorphism and the difficulty of sample preparation. To establish the relationship between λ-ET and λ-BEDSe in the universal phase diagram and reveal the electronic phases at higher pressures than AF state, we are currently conducting NMR experiments under pressure on λ-BEDSe.

We mention the availability of various λ-D_2MCl$_4$. Table V shows the combinations of donor molecule D and anions M = Ga and Fe along with the ground states of the compounds and the ease of obtaining λ-type salts (whether polymorphs are obtained simultaneously). λ-(BETS)$_2M$Cl$_4$ and λ-(STF)$_2M$Cl$_4$ are obtained together with the κ phase [71, 72], but they are easy to distinguish because of their different crystal shapes. In contrast, λ-ET is difficult to distinguish from the δ-type salt, and the λ phase is a minor product [35–37], which hampers the study of the AF phase using polycrystalline samples such as in μSR measurements. We found that λ-BEDSe can be synthesized without other polymorphs, and this enabled the detailed measurements in the present study. It has recently been demonstrated that the electronic system can be observed by polycrystalline ^{69,71}Ga-NMR measurements on λ-BETS [73]; these experiments are easy to perform even under pressure, and therefore, λ-BEDSe is also suitable for such experiments.

TABLE V. Ground state and crystal preparation of λ-D_2MCl$_4$ (D = BETS, BEDT-STF, BEDT-TTF, BEDSe-TTF and M = Ga, Fe).

	$GaCl_4^-$	$FeCl_4^-$
BETS	◯ SC	◯ AF (FISC)
BEDT-STF	◯ PI	(◯) AF
BEDT-TTF	△ AF	×
BEDSe-TTF	◎ AF	◎ AF

◯: mixture of the λ and κ phases, whereas κ-(STF)$_2$FeCl$_4$ has not been reported; ◎: λ phase only; △: δ' and λ phases (λ: minor product); ×: not reported

λ-(BETS)$_2$FeCl$_4$ exhibits a field-induced superconductivity [12] and a strange metal–insulator transition with AF ordering [74], whereas λ-(STF)$_2$FeCl$_4$ shows a unique magnetic response, in which the magnetization processes between π and 3d spin systems are different in the AF state [32–34]. In these Fe-containing systems, the π–d interaction plays an essential role in the physical properties. To understand the donor molecule substitution effect of the π–d interaction, we are interested in the magnetic properties at the more negative pressure side, but the λ-(ET)$_2$FeCl$_4$ has not been reported. λ-(BEDSe-TTF)$_2$FeCl$_4$, which is another possible salt located on the low pressure side, has been reported by Cui *et al.*, and magnetic susceptibility measurements suggest that it is paramagnetic down to 4 K [40]. However, our research group has recently found that λ-(BEDSe-TTF)$_2$FeCl$_4$ exhibits an AF transition with a different magnetic process between π and 3d spin systems [75]. The result that λ-BEDSe without 3d spins shows antiferromagnetism would be an important finding for the discussion of the π–d interaction mechanism in λ-(BEDSe-TTF)$_2$FeCl$_4$.

IV. SUMMARY

We investigated the structural and magnetic properties of λ-BEDSe to determine whether this material can be placed on the universal phase diagram of λ-D_2GaCl$_4$. The systematic band calculations for D = BEDSe-TTF, BEDT-TTF, and BETS salts suggested that λ-BEDSe is a Mott insulator as well as λ-ET and that there is a Mott transition between them and λ-BETS. Further, we found that the network of J in the λ-BEDSe salt consists of a combination of triangular and square lad-

ders. The broad peaks observed in the temperature dependence of $\chi_{\rm spin}$ are intermediate between those in the triangular and square lattice Heisenberg AF spin models, which is consistent with the network of J. From a microscopic viewpoint, the development of the internal magnetic fields was observed from muon precession signals, which is definitive evidence that λ-BEDSe exhibits AF ordering. In the ^{13}C-NMR measurement, we observed the divergent behavior of $(T_1T)^{-1}$ towards 22 K, below which the NMR spectra split discretely, retaining the central peak, as observed in λ-ET. These behaviors are qualitatively the same as those of λ-ET, which sugges that both salts are in the same electronic phase in the universal phase diagram of λ-type salts. Further, λ-BEDSe can be synthesized without polymorphism, unlike λ-ET. These features and the present results promote the understanding of the nature of the electronic states located at lower pressure than the SC phase in the phase diagram, e.g., whether the nonmagnetic ordered phase between the AF and SC phases is intrinsic by the experiments under pressure.

ACKNOWLEDGMENTS

The authors would like to thank Prof. R. Kato for his advice on the synthesis of the BEDSe-TTF molecule. This work was partly supported by Hokkaido University, Global Facility Center (GFC), Advanced Physical Property Open Unit (APPOU), funded by MEXT under "Support Program for Implementation of New Equipment Sharing System" (JPMXS0420100318). This work was also partially supported by the Japan Society for the Promotion of Science KAKENHI Grant Numbers 20K14401, 19K03758, and 21K03438.

[1] A. Andrieux, D. Jérome, and K. Bechgaard, Journal de Physique Lettres **42**, 87 (1981).
[2] A. Kawamoto, K. Miyagawa, Y. Nakazawa, and K. Kanoda, Physical Review B **52**, 15522 (1995).
[3] K. Miyagawa, A. Kawamoto, Y. Nakazawa, and K. Kanoda, Physical Review Letters **75**, 1174 (1995).
[4] M. Ito, T. Uehara, H. Taniguchi, K. Satoh, Y. Ishii, and I. Watanabe, Journal of the Physical Society of Japan **84**, 053703 (2015).
[5] D. Jérome, A. Mazaud, M. Ribault, and K. Bechgaard, Journal de Physique Lettres **41**, 95 (1980).
[6] J. M. Williams, A. M. Kini, H. H. Wang, K. D. Carlson, U. Geiser, L. K. Montgomery, G. J. Pyrka, D. M. Watkins, and J. M. Kommers, Inorganic Chemistry **29**, 3272 (1990).
[7] S. Brown, Physica C: Superconductivity and its Applications **514**, 279 (2015).
[8] K. Bechgaard, K. Carneiro, M. Olsen, F. B. Rasmussen, and C. S. Jacobsen, Physical Review Letters **46**, 852 (1981).
[9] H. Urayama, H. Yamochi, G. Saito, K. Nozawa, T. Sugano, M. Kinoshita, S. Sato, K. Oshima, A. Kawamoto, and J. Tanaka, Chemistry Letters **17**, 55 (1988).
[10] A. M. Kini, U. Geiser, H. H. Wang, K. D. Carlson, J. M. Williams, W. K. Kwok, K. G. Vandervoort, J. E. Thompson, and D. L. Stupka, Inorganic Chemistry **29**, 2555 (1990).
[11] M. Lang and J. Müller, Organic superconductors, in *The Physics of Superconductors* (Springer, 2004) pp. 453–554.
[12] S. Uji, H. Shinagawa, T. Terashima, T. Yakabe, Y. Terai, M. Tokumoto, A. Kobayashi, H. Tanaka, and H. Kobayashi, Nature **410**, 908 (2001).
[13] M. A. Tanatar, T. Ishiguro, H. Tanaka, and H. Kobayashi, Physical Review B **66**, 134503 (2002).
[14] W. A. Coniglio, L. E. Winter, K. Cho, C. C. Agosta, B. Fravel, and L. K. Montgomery, Physical Review B **83**, 224507 (2011).
[15] S. Uji, K. Kodama, K. Sugii, T. Terashima, T. Yamaguchi, N. Kurita, S. Tsuchiya, T. Konoike, M. Kimata, A. Kobayashi, B. Zhou, and H. Kobayashi, Journal of the Physical Society of Japan **84**, 104709 (2015).
[16] L. Balicas, J. S. Brooks, K. Storr, S. Uji, M. Tokumoto, H. Tanaka, H. Kobayashi, A. Kobayashi, V. Barzykin, and L. P. Gor'kov, Physical Review Letters **87**, 067002 (2001).
[17] S. Imajo, N. Kanda, S. Yamashita, H. Akutsu, Y. Nakazawa, H. Kumagai, T. Kobayashi, and A. Kawamoto, Journal of the Physical Society of Japan **85**, 043705 (2016).
[18] S. Imajo, S. Yamashita, H. Akutsu, H. Kumagai, T. Kobayashi, A. Kawamoto, and Y. Nakazawa, Journal of the Physical Society of Japan **88**, 023702 (2019).
[19] T. Kobayashi, H. Taniguchi, A. Ohnuma, and A. Kawamoto, Physical Review B **102**, 121106(R) (2020).
[20] H. Kobayashi, H. Akutsu, E. Arai, H. Tanaka, and A. Kobayashi, Physical Review B **56**, R8526 (1997).
[21] H. Tanaka, A. Kobayashi, A. Sato, H. Akutsu, and H. Kobayashi, Journal of the American Chemical Society **121**, 760 (1999).
[22] T. Kobayashi, T. Ishikawa, A. Ohnuma, M. Sawada, N. Matsunaga, H. Uehara, and A. Kawamoto, Physical Review Research **2**, 023075 (2020).
[23] H. Tanaka, A. Kobayashi, T. Saito, K. Kawano, T. Naito, and F. H. Kobayashi, Advanced Materials **8**, 812 (1996).
[24] H. Mori, T. Okano, M. Kamiya, M. Haemori, H. Suzuki, S. Tanaka, Y. Nishio, K. Kajita, and H. Moriyama, Physica C **357-360**, 103 (2001).
[25] The relative positions between λ-ET and λ-STF and between λ-STF and λ-BETS were determined from the pressure variation of the temperature dependence of electrical resistivity [24] and the pressure dependence of superconducting transition temperature T_c [21,27], respectively.
[26] D. Jérome, Science **252**, 1509 (1991).
[27] T. Minamidate, Y. Oka, H. Shindo, T. Yamazaki, N. Matsunaga, K. Nomura, and A. Kawamoto, Journal of the Physical Society of Japan **84**, 063704 (2015).
[28] Y. Saito, S. Fukuoka, T. Kobayashi, A. Kawamoto, and H. Mori, Journal of the Physical Society of Japan **87**, 013707 (2018).

[29] Y. Saito, N. H., S. M., T. Yamazaki, S. Fukuoka, N. Matsunaga, K. Nomura, M. Dressel, and A. Kawamoto, (2019), arXiv:1910.09963 [cond-mat.str-el].

[30] H. Akutsu, E. Arai, H. Kobayashi, H. Tanaka, A. Kobayashi, and P. Cassoux, Journal of the American Chemical Society **119**, 12681 (1997).

[31] Y. Oshima, H. Cui, and R. Kato, Magnetochemistry **3**, 10 (2017).

[32] T. Minamidate, H. Shindo, Y. Ihara, A. Kawamoto, N. Matsunaga, and K. Nomura, Physical Review B **97**, 104404 (2018).

[33] S. Fukuoka, M. Sawada, T. Minamidate, N. Matsunaga, K. Nomura, Y. Ihara, A. Kawamoto, Y. Doi, M. Wakeshima, and Y. Hinatsu, Journal of the Physical Society of Japan **87**, 1 (2018).

[34] S. Fukuoka, T. Minamidate, Y. Ihara, and A. Kawamoto, Physical Review B **101**, 184402 (2020).

[35] L. V. Zorina, S. S. Khasanov, B. Z. Narymbetov, R. P. Shibaeva, A. I. Kotov, and É. B. Yagubskii, Crystallography Reports **46**, 219 (2001).

[36] B. Zhang and Y. Zhang, Crystals **3**, 112 (2013).

[37] M. Kurmoo, P. Day, P. Guionneau, G. Bravic, D. Chasseau, L. Ducasse, M. L. Allan, I. D. Marsden, and R. H. Friend, Inorganic Chemistry **35**, 4719 (1996).

[38] T. Mallah, C. Hollis, S. Bott, M. Kurmoo, P. Day, M. Allan, and R. H. Friend, Journal of the Chemical Society, Dalton Transactions , 859 (1990).

[39] B. Zhang, M. Kurmoo, T. Mori, Y. Zhang, F. L. Pratt, and D. Zhu, Crystal Growth & Design **10**, 782 (2010).

[40] H. B. Cui, S. Otsubo, Y. Okano, and H. Kobayashi, Chemistry Letters **34**, 254 (2005).

[41] J. Sakata, H. Sato, A. Miyazaki, T. Enoki, Y. Okano, and R. Kato, Solid State Communications **108**, 377 (1998).

[42] G. M. Sheldrick, Acta Crystallographica Section A Foundations and Advances **71**, 3 (2015).

[43] G. M. Sheldrick, Acta Crystallographica Section C Structural Chemistry **71**, 3 (2015).

[44] T. Mori, A. Kobayashi, Y. Sasaki, H. Kobayashi, G. Saito, and H. Inokuchi, Bulletin of the Chemical Society of Japan **57**, 627 (1984).

[45] M. H. Whangbo, W. M. Walsh, R. C. Haddon, and F. Wudl, Solid State Communications **43**, 637 (1982).

[46] P. M. Grant, Physical Review B **26**, 6888 (1982).

[47] T. Mori and M. Katsuhara, Journal of the Physical Society of Japan **71**, 826 (2002).

[48] The ξ exponent (ionization potential (eV)) for atomic orbitals are as follows. Se : 4d 2.44 (-20.0), 4p 2.07 (-10.8), 4s 1.5 (-5.44). S : 3d 2.122 (-20.0), 3p 1.827 (-11.0), 3s 1.5 (-5.44). C : 2p 1.625 (-21.4), 2s 1.625 (-11.4). H : 1s 1.3 (-13.6).

[49] H. H. Wang, L. K. Montgomery, U. Geiser, L. C. Porter, K. D. Carlson, J. R. Ferraro, J. M. Williams, C. S. Cariss, and R. L. Rubinstein, Chemistry of Materials **1**, 140 (1989).

[50] A. Kawamoto, M. Yamashita, and K.-I. Kumagai, Physical Review B **70**, 212506 (2004).

[51] M. Matsumoto, H. Kato, Y. Kuwata, A. Kawamoto, N. Matsunaga, and K. Nomura, Journal of the Physical Society of Japan **81**, 114709 (2012).

[52] G. E. Pake, The Journal of Chemical Physics **16**, 327 (1948).

[53] T. Mori, H. Mori, and S. Tanaka, Bulletin of the Chemical Society of Japan **72**, 179 (1999).

[54] C. Hotta, Journal of the Physical Society of Japan **72**, 840 (2003).

[55] K. Kanoda, Hyperfine Interactions **104**, 235 (1997).

[56] N. Yoneyama, A. Miyazaki, T. Enoki, and G. Saito, Bulletin of the Chemical Society of Japan **72**, 639 (1999).

[57] M. Tamura and R. Kato, Journal of Physics: Condensed Matter **14**, L729 (2002).

[58] M. Lines, Journal of Physics and Chemistry of Solids **31**, 101 (1970).

[59] K. Sakakida and H. Shimahara, Journal of the Physical Society of Japan **86**, 124709 (2017).

[60] H. Seo and H. Fukuyama, Journal of the Physical Society of Japan **66**, 3352 (1997).

[61] H. Aizawa, T. Koretsune, K. Kuroki, and H. Seo, Journal of the Physical Society of Japan **87**, 093701 (2018).

[62] D. P. Sari, R. Asih, K.-i. Hiraki, T. Nakano, Y. Nozue, Y. Ishii, A. D. Hillier, and I. Watanabe, Physical Review B **104**, 224506 (2021).

[63] R. Ishikawa, H. Tsunakawa, K. Oinuma, S. Michimura, H. Taniguchi, K. Satoh, Y. Ishii, and H. Okamoto, Journal of the Physical Society of Japan **87**, 064701 (2018).

[64] G. Kresse and J. Furthmüller, Physical Review B **54**, 11169 (1996).

[65] G. Kresse and J. Furthmüller, Computational Materials Science **6**, 15 (1996).

[66] J. P. Perdew, K. Burke, and M. Ernzerhof, Physical Review Letters **77**, 3865 (1996).

[67] D. F. Smith, C. P. Slichter, J. A. Schlueter, A. M. Kini, and R. G. Daugherty, Physical Review Letters **93**, 167002 (2004).

[68] F. Kagawa, Y. Kurosaki, K. Miyagawa, and K. Kanoda, Physical Review B **78**, 184402 (2008).

[69] C. Yasuda, S. Todo, K. Hukushima, F. Alet, M. Keller, M. Troyer, and H. Takayama, Physical Review Letters **94**, 217201 (2005).

[70] M. Sawada, Ph.D. thesis, Hokkaido University (2021).

[71] A. Kobayashi, T. Udagawa, H. Tomita, T. Naito, and H. Kobayashi, Chemistry Letters , 2179 (1993).

[72] T. Naito, H. Kobayashi, and A. Kobayashi, Bulletin of the Chemical Society of Japan **70**, 107 (1997).

[73] T. Kobayashi, K. Tsuji, A. Ohnuma, and A. Kawamoto, Physical Review B **102**, 235131 (2020).

[74] H. Akiba, S. Nakano, Y. Nishio, K. Kajita, B. Zhou, A. Kobayashi, and H. Kobayashi, Journal of the Physical Society of Japan **78**, 033601 (2009).

[75] R. Saito, Y. Iida, T. Kobayashi, H. Taniguchi, N. Matsunaga, S. Fukuoka, and A. Kawamoto, Physical Review B **105**, 165115 (2022).